analytical chemistry

pubs.acs.org/ac Article

Biomimetic Molecular Clamp Nanopores for Simultaneous Quantifications of NAD$^+$ and NADH

Xingtong Liu, Wanyue Feng, Fujun Yao, Jinlei Zhang, Rauf Ayesha, Tingting Chen, Xiaoyu Shi, Xixi Qiao, Luping Ma, Sha Yu, and Xiao-feng Kang*

Cite This: *Anal. Chem.* 2021, 93, 7118−7124 Read Online

ACCESS | Metrics & More | Article Recommendations | Supporting Information

ABSTRACT: NADH/NAD$^+$ is pivotal to fundamental biochemistry research and molecular diagnosis, but recognition and detection for them are a big challenge at the single-molecule level. Inspired by the biological system, here, we designed and synthesized a biomimetic NAD$^+$/NADH molecular clamp (MC), octakis-(6-amino-6-deoxy)-γ-cyclomaltooctaose, and harbored in the engineered α-HL(M113R)$_7$ nanopore, forming a novel single-molecule biosensor. The single-molecule measurement possesses high selectivity and a high signal-to-noise ratio, allowing to simultaneously recognize and detect for sensing NADH/NAD$^+$ and their transformations.

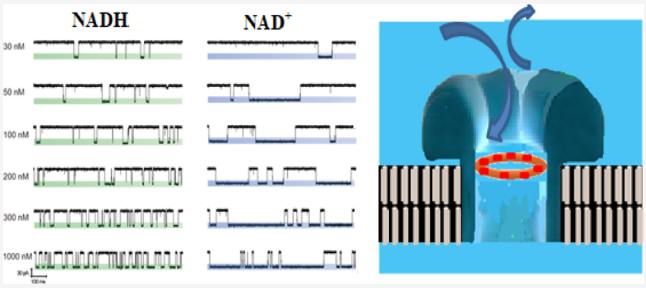

Biological systems are incredibly complex involving intrinsic heterogeneity, a combination of multiple stochastic events, catalytic transforms, and so forth.[1−4] To address problems in such complex systems, the innovation in single-molecule biotechnology is imperative. As opposed to bulk techniques where readouts/measurements result from averaging of properties of multiple molecules, single-molecule studies can track individual biomolecules in space and time. More importantly, this method owns unique capability to simultaneously output fingerprint information of not only same molecules but also many different molecules. The single-molecule recording to capture the characteristic details of sample heterogeneity is very suitable for applications in biological systems, especially in the detections of complex biofluids and/or those components with minor differences.

Nicotinamide adenine dinucleotide (reduced, NADH; oxidized, NAD$^+$) is an important pyridine nucleotide that functions as a key cofactor in eukaryotic cells and plays an extremely crucial role in the production of energy through redox reaction. The NADH/NAD$^+$ redox as a major carrier of H$^+$ and e$^-$ in living systems is required in over 500 enzymatic reactions including various dehydrogenases, reductases, and hydroxylases.[5] The NADH/NAD$^+$ ratio can serve as a pivotal indicator that reflects the overall redox state of many physiological or pathological processes, such as the energy metabolism, mitochondrial functions, calcium homeostasis, gene expression, cell death, embryonic development, blood flow, aging, cancer, and diabetes,[6−11] but the extent to which it reflects versus drives metabolic physiology *in vivo* is poorly understood,[12] which is largely because of the technical limit for detecting NADH/NAD$^+$ at the molecular level. Numerous methods have been developed and used for detecting NAD$^+$ and NADH, such as electrochemistry and fluorescence.[13−16] Although highly sensitive and selective, the electrochemical oxidation of NADH requires the modification of the solid electrodes to lower its high overpotential. The fluorescence assay usually involved complex genetically encoded proteins and nanoparticles. Moreover, the results provided by these methods have mostly been based on the ensemble averaging. Thus, to obtain insight into these essential and complex biological processes and to meet clinical molecular diagnosis, there is a high demand to simultaneously detect them, however, which is a big challenge due to similar structures (only one hydride difference), fast transformation under specific enzymes,[17] possible multi-process involvement, and wider cell dynamic distribution (nM to μM).[5]

Among available single-molecule tool boxes, nanopore technology has distinctive advantages for exploring biological problems, for example, direct detection in solution, easy operation, the simplest and label-free assay, and so forth.[18−22] In principle, the technology is based on the spiking current generated by the analyte blocking the pore. To generate analytical signals, it is necessary for the nanopore to match the size of the analyte. Therefore, when sensing small biomolecules, protein nanopores should be preferred over solid nanopores. However, even with comparable dimensions,

Received: March 5, 2021
Accepted: April 13, 2021
Published: April 27, 2021

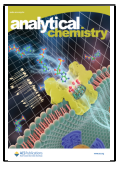

https://doi.org/10.1021/acs.analchem.1c00986
Anal. Chem. 2021, 93, 7118−7124

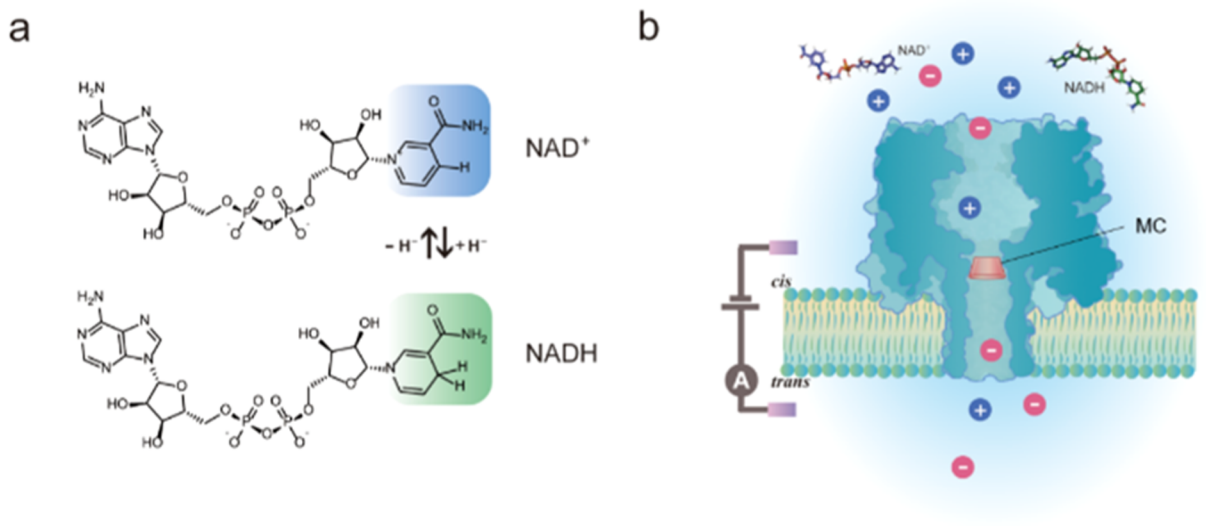

Figure 1. (a) Interconversion of NAD^+ and NADH; (b) schematic diagram of the αHL-$(M113R)_7$/MC nanopore biosensor.

effective protein nanopores including the most commonly used α-hemolysin (α-HL) remain unpredictable, which are largely because of a shortage of pore selectivity. Although some strategies have been reported to improve it, such as functionalizing the nanopore surface with hydrophobic[23] or positively[24] or negatively[25] charged residues, modifying,[26] or carrying the analyte,[27−29] these methods require careful optimization, and there are only very limited improvements, which are ineffective. Furthermore, the biological modification of the nanopore involves a complicated and costly bioengineering process. To achieve high validity and specificity, designing and synthesizing chemical recognition molecules could simply and cheaply provide an alternative solution.

In this study, we developed molecular clamp nanopore sensor to simultaneously detect NADH and NAD^+. Inspired by the biological system and considering the matching with the protein nanopore, we designed and synthesized an artificial molecule, octakis-(6-amino-6-deoxy)-γ-cyclomaltooctaose, which can well recognize NADH/NAD^+. When embedding it in the mutated α-HL$(M113R)_7$ nanopore, a single-molecule molecular clamp (MC) for NADH/NAD^+ was thus formed (Figure 1). We show that the nanopore sensor can selectively and sensitively obtain the fingerprint information of NADH and NAD^+. The exceptional capability with single-hydride resolution was demonstrated through the single-molecule electronic measurements in both simultaneously recognizing NADH/NAD^+ and real-time enzyme-catalyzing transformation kinetics.

EXPERIMENTAL SECTION

Reagents and Materials. β-Nicotinamide adenine dinucleotide, reduced disodium salt hydrate (NADH, ≥97.0%), β-nicotinamide adenine dinucleotide hydrate (NAD^+, ≥99%), and alcohol dehydrogenase from saccharomyces cerevisiae (≥300 units/mg) were purchased from Sigma-Aldrich. Bovine serum albumin (BSA, Genview), human serum albumin (HSA, Yobios), bovine insulin (yuanye Bio-Technology), and hemoglobin (Sigma-Aldrich) were used as received without further purification. Lipid 1,2-diphytanoyl-*sn*-glycero-3-phosphocholine (DPhPC) was obtained from Avanti Polar Lipids. Teflon film (thickness: 25 μm) was from Good Fellow.

Synthesis of Recognizable Molecules. Total synthesizing routes of octakis-(6-amino-6-deoxy)-γ-cyclomaltooctaose (compound 4) are shown in Figure S1. First, octakis-(6-azido-6-deoxy)-γ-cyclomaltooctaose (compound 3) was prepared from γ-cyclomaltooctaose (compound 1) according to the literature;[30,31] then, compound 4 was produced by the reaction of compound 3 and Ph3P. The details of last step are as follows: 0.53 g of compound 3 was added in 10 mL of dry DMF containing 1.6 g of Ph3P to react for 1 h at room temperature; next, 25% NH3 solution was added dropwise, and the solution became a white suspension; further stirring was carried out at room temperature for 18 h; after removing the solvent by reduced pressure distillation, EtOH was added; the precipitate was collected by filtration and washed repeatedly by EtOH; the obtained precipitate was acidified by HCl solution until the pH had reached 6; finally, the yellow solid (0.40 g, 87%) was collected and analyzed (Figure S2). ESI-MS m/z: $[M + 2H]^{2+}$ 645.2903, $[M + 3H]^{3+}$ 430.5303.

Preparation of α-HL$(M113R)_7$ Protein Nanopores. The mutant α-HL M113R (Met-113 → Arg) was made by cutting pT7-HL-RL2 with SacII and HpaI and displacing the original internal fragment with duplex DNA formed from 5-GAATTCGATTGATACAAAAGAGTATAGAAGTACGTT-3(sense) and 5-AACGTACTTCTATACTCTTTTTAT-CAATCGAATTCCGC-3(antisense). The mutant was constructed in an RL2 background, and thus, each mutant contains the following additional replacements with respect to WT-HL: Lys-8 → Ala, Val-124 → Leu, Gly-130 → Ser, Asn-139 → Gln, and Ile-142 → Leu. The mutant α-HL M113R protein synthesized *in vitro* by coupled transcription and translation (IVTT) was assembled into homoheptamers by the inclusion of rabbit red cell membranes (rRBCM) during synthesis. The heptamers were purified by sodium dodecyl sulfate-polyacrylamide gel electrophoresis and stored in aliquots at −80 °C. The mutant polypeptides were synthesized and purified twice.

Single-Channel Recording and Data Analysis. A lipid bilayer of DPhPC was formed on a 130−150 μm orifice in a 25 μm thick Teflon septum that separated the cis and trans compartments (1.5 mL each) of a planar bilayer apparatus. The cis compartment was connected to the ground. The electrolyte in both chambers was 10 mM Tris buffer containing

https://doi.org/10.1021/acs.analchem.1c00986
Anal. Chem. 2021, 93, 7118−7124

1 M KCl (pH 7.4). Mutant homoheptameric pore protein was added to the cis compartment to a final concentration of 0.2−2.0 ng mL^{-1}. NAD^+ and NADH were added into the cis chamber, and octakis-(6-amino-6-deoxy)-γ-cyclomaltooctaose was added into the trans chamber. Unless otherwise stated, all experiments were completed at 20 ± 1 °C and +120 mV. Single-channel currents were recorded with a patch clamp amplifier (Axopatch 200B, Molecule Devices). The signal was low-pass-filtered with a built-in 4-pole Bessel filter at 5 kHz and sampled at 20 kHz with a computer equipped with a Digidata 1440A A/D converter (Molecule Devices). Data were analyzed and prepared for presentation by using pClamp 10.5 software (Axon Instruments) and Origin 9.0 (MicroCal Northampton, MA). Current amplitudes were obtained from the peaks of all-point histograms. Kinetic constants were calculated by using $k_{off} = 1/\tau_{off}$, $k_{on} = 1/(\tau_{on}[A])$, and $K_f = k_{on}/k_{off}$, where $[A]$ is the concentration of NADH or NAD^+.

RESULTS AND DISCUSSION

Design of the NAD^+/NADH Molecular Clamp. Sirtuins are evolutionarily conserved NAD^+ or NADH-dependent lysine deacetylases. These cellular enzymes are metabolic sensors sensitive to NAD^+/NADH levels that maintain physiological homeostasis in the animal and plant cells.[32,33] Sirtuin, such as Sir2 as shown in Figure S3, shares a catalytic core with two domains, a large NAD^+-binding domain with a Rossmann fold and a small Zn^{2+}-binding domain, and forms a hydrophobic channel pocket that can bind the acetylated lysine with free side-chain NH_2 between the two domains. The functional key to sirtuin to recognize NAD^+/NADH is the hydrophobic channel and the positively charged amino residues. Inspired by the specific structure, we designed and synthesized a biomimetic NAD^+/NADH molecular clamp (MC), octakis-(6-amino-6-deoxy)-γ-cyclomaltooctaose, containing a hydrophobic hollow and a positively charged cluster (Figure S1). The cavity internal diameter (7.5−8.3 Å) is comparable with the size of the NADH molecule with 5.3−7.7 Å in the dynamic diameter (Figure S4), and the external diameter (about ∼17.5 Å) matches well with the size of the α-HL $(M113R)_7$ nanopore (the minimum diameter of 14 Å at the constriction site, the β-barrel with a vestibule of a 26 Å internal diameter).

Interactions between MC and NAD(H) in the Bulk Solution. The ability of octakis-(6-amino-6-deoxy)-γ-cyclomaltooctaose as a molecular trap to catch NAD(H) was explored experimentally. The predefined property was demonstrated by forming MC-NAD(H) complexes in the bulk solution (for details, see Supporting Information 4). By measuring UV−visible absorbance (ΔA) at 260 nm, we obtained their values of the formation constant K_f and the standard Gibbs free energy Δ$G°$: K_f (MC-NADH) = 2.20 × 10^4 M^{-1}, K_f (MC-NAD^+) = 7.56 × 10^3 M^{-1}, Δ$G°$(MC-NADH) = −24.36 kJ·mol^{-1}, and Δ$G°$(MC-NAD^+) = −21.76 kJ·mol^{-1} for NAD^+ (Tables S1 and S2). Compared with NAD^+, NADH has a stronger interaction with MC, which should be attributed to their molecular charges (NAD^+: only one net negative charge, NADH: two net negative charges).

We further used molecular simulation (for details, see Supporting Information 5) to evaluate the interaction between MC and NAD(H). The simulation analysis revealed that NADH and NAD^+ all displayed high affinity with MC. Two complexes had the same salt bridge number (NADH-MC: 2; NAD^+-MC: 2); however, the number of hydrogen bonds was significantly distinct (NADH-MC: 6, NAD^+-MC: 3) (see Figure S6). The grid score (Table S3) suggests that the difference in the binding affinity comes mainly from the electrostatic force. The conclusion is consistent with the experimental results.

Single-Molecule Recognition and Detection for NADH and NAD^+. A genetically engineered protein α-HL$(M113R)_7$ nanopore was prepared and bound MC molecules through an arginine ring at residue 113 sites, forming a single-molecule NADH/NAD^+ biosensor. Single-channel electronic recording showed that the α-HL$(M113R)_7$ pore in 1.0 M KCl created a stable opening current level: 121 ± 5 pA (n = 15) at +120 mV (Figure 2a). After binding MC, the channel current became 67 ± 3 pA (n = 15) (Figure 2b). Compared molecular binding in the α-HL $(M113R)_7$ pore, the MC molecule is 8700 times stronger than γ-cyclomaltooctaose (see Table S4 and Figure S7 in Supporting Information 6). When adding NADH or NAD^+ to the cis side (on the opposite side of MC), two distinct blocking events were formed (Figure 2c,e). The values of $I_{res\%}$ are 6.78 ± 0.02 for NADH and 7.41 ± 0.01 for NAD^+, respectively (Figure S8a,b). Here, the residual current percentage is defined as $I_{res\%} = I/I_0 \times 100$, where I is the residual current and I_0 is the open pore current. Single

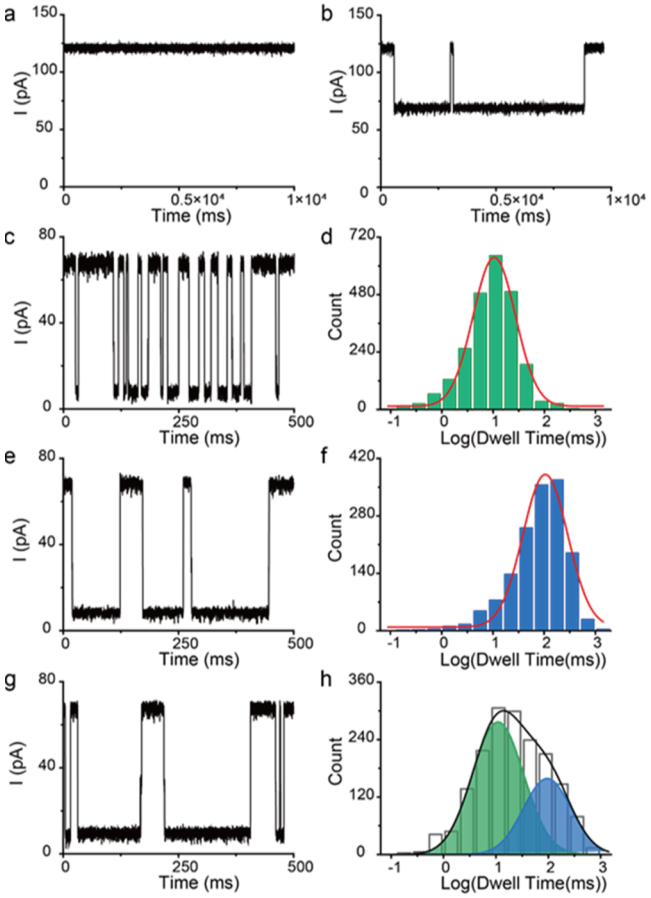

Figure 2. Typical single-channel recordings for (a) αHL-$(M113R)_7$ pore, (b) αHL-$(M113R)_7$-MC pore, (c) NADH in the αHL-$(M113R)_7$-MC pore, (e) NAD^+ in the αHL-$(M113R)_7$-MC pore, and (g) NAD^+ (250 nM) and NADH (100 nM) mixture in the αHL-$(M113R)_7$-MC pore. The semilogarithmic histograms of dwell time for NADH (d), NAD^+ (f), and the mixture (h). The MC concentration is 2 μM. The applied potential is +120 mV.

https://doi.org/10.1021/acs.analchem.1c00986
Anal. Chem. 2021, 93, 7118−7124

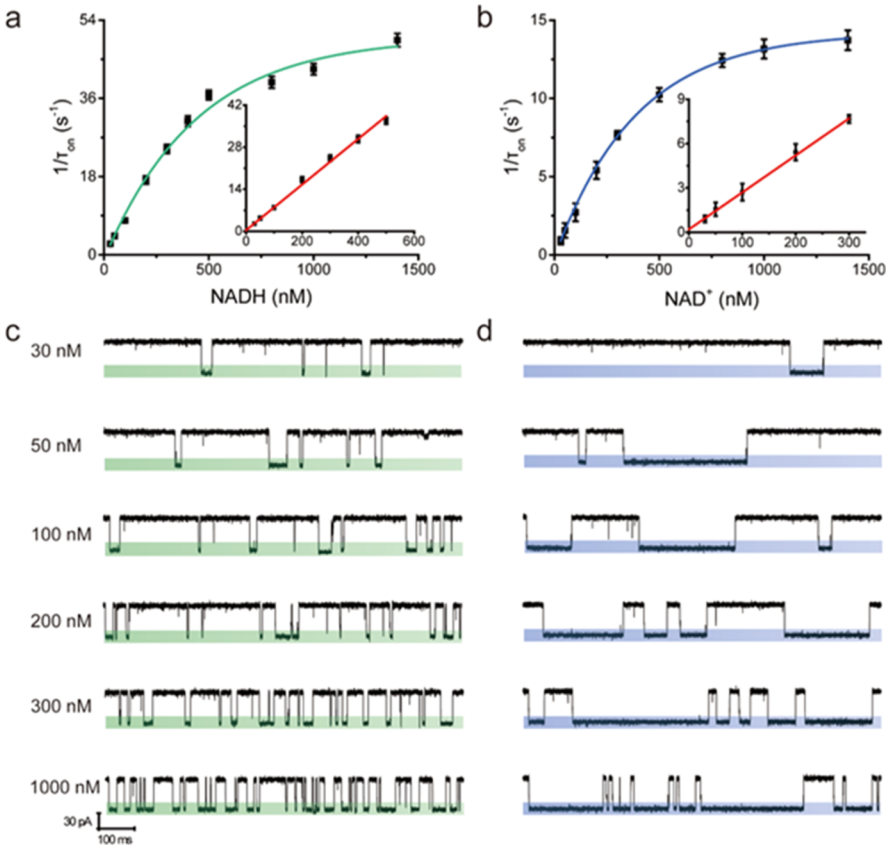

Figure 3. Concentration-dependent event frequency: (a) plots of event frequency vs NADH concentrations. The inset is the linear relationship in the range of 30−500 nM; (b) plots of event frequency vs NAD^+ concentrations. The inset is the linear relationship in the range of 30−300 nM. (c,d) Representative current traces of NADH (left) and NAD^+ (right) at different concentrations.

hydride change between NADH and NAD^+ results in 0.63 of current percentage difference. Surprisingly, the dwell time is the reverse of the current trend: 10.47 ± 1.05 ms for NADH and 104.71 ± 1.07 ms for NAD^+ (Figure 2d,f). Such a large retention difference in the pore is an important indicator of their identity, reflecting their distinct interactions with the pore. This difference should be mainly related to both their molecular charges (NAD^+: only one net negative charge, NADH: two net negative charges) and the volume size [see Supporting Information 3 and Figure S4b: V(NADH) = 596.81 Å^3, $V(NAD^+)$ = 583.83 Å^3]. Control experiments demonstrated that negatively charged proteins did not generate any blocking signals and interferences (Figure S9).

Next, we assessed the discriminating ability for NADH and NAD in the mixture. When NADH and NAD^+ were simultaneously added to the cis side, the αHL-$(M113R)_7$-MC pore instantly produced their corresponding blocking characteristics that were the same as those of the individual substance (Figure 2g,h), showing a good resolution for NAD^+ and NADH in the mixture.

According to their characteristics, we chose the cutoff range of NADH and NAD^+ events (2−14 ms for NADH dwell time, ≥45 ms for NAD^+ dwell time) and demonstrated that the event frequency and the corresponding concentration (30−500 nM for NADH, 30−300 nM for NAD^+) had a good linear relationship (Figure 3): $f_{NADH} = 0.076C_{NADH} + 0.372$ with $R^2 = 0.996$; $f_{NAD^+} = 0.025C_{NAD^+} + 0.153$ with $R^2 = 0.999$. The detection limit (S/N = 3) is 5 nM for NADH and 6.4 nM for NAD^+.

Binding Kinetics in the Confined Nanopore. The association/dissociation equilibrium of NADH and NAD^+ in the αHL$(M113R)_7$-MC nanopore was studied by a voltage-dependent model and analysis (for details, see Supporting Information 8). As shown in Figure S10, the formation constant ($K_f = k_{on}/k_{off}$) and the standard Gibbs free energy ΔG° [$\Delta G^\circ = -RT \ln(K_f)$] for NADH gradually decreased with increasing voltage. Interestedly, the ΔG° for NAD^+ exhibited a U-shape voltage dependence. Based on corresponding model, the obtained standard free energy at 0 mV ($\Delta G^\circ_{v=0}$) was −35.07 kJ mol^{-1} for NADH and −17.06 kJ mol^{-1} for NAD^+. These values are significantly different from ΔG° in the bulk solution, which should be ascribed to the space effect in the confined nanopore.

Real-Time Monitoring of Enzyme-Catalyzed Conversion. Alcohol dehydrogenase (ADH, EC1.1.1.1, from *Saccharomyces cerevisiae*) can catalyze ethanol to produce ethanal, while NAD^+ is reduced to NADH (Figure 4a). Based on the above method, the catalytic reaction process was real-time-monitored. Excess ethanol (30 μL), 200 nM NAD^+, and 2.5 unit/mL ADH were added into the cis chamber. In the absence of ADH or t = 0, only the signal for NAD^+ was observed (Figure 4b). As the reaction progressed, the NADH signal appeared, and finally, all NAD^+ completely converted to NADH after 20 min (Figure 4b−e). The transformation of the analyte in the process was clearly observed by visualizing the semilogarithmic histogram of dwell time (Figure 4f−i) and the concentration changes (Figure 4j). The reaction had a faster rate during first 7 min, followed by a slow process. The apparent rate constant was (8.9 ± 0.1) × 10^{-4} min^{-1}.

https://doi.org/10.1021/acs.analchem.1c00986
Anal. Chem. 2021, 93, 7118−7124

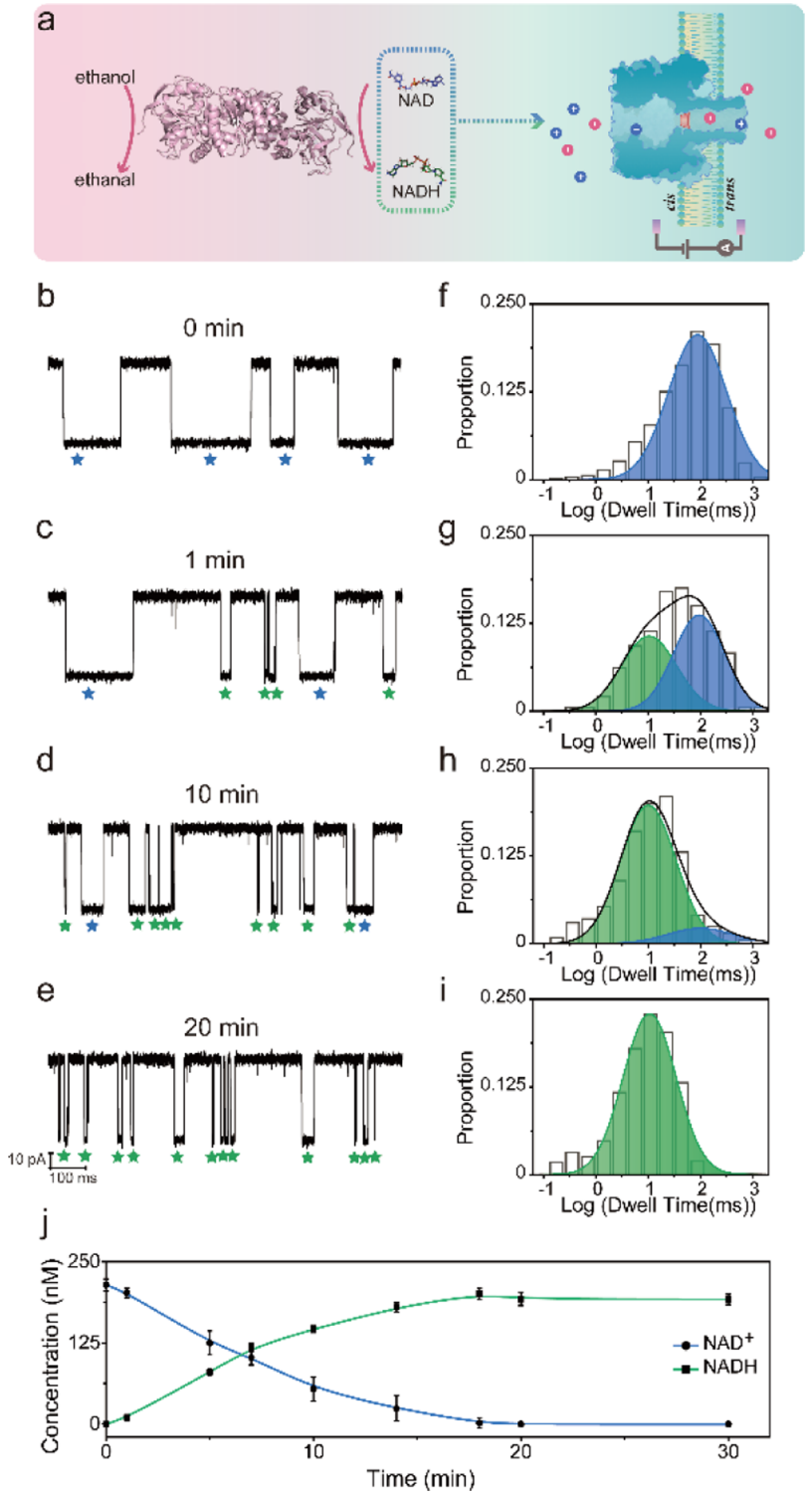

Figure 4. Enzyme catalytic conversion of NAD^+: (a) schematic diagram of enzyme-catalyzed conversion of NAD^+; (b–e) single-channel current traces at 0, 1, 10, and 20 min; (f–i) semilogarithmic histogram of dwell time at 0, 1, 10, and 20 min; (j) concentration variations of NAD(H) during the catalytic reaction.

CONCLUSIONS

In summary, this paper successfully constructed the αHL-$(M113R)_7$-MC nanopore sensor for recognizing and detecting NADH and NAD^+ as well as their transformations. The single-molecule approach has high selectivity that allows the MC nanopore to effectively capture and identify NADH and NAD^+. Being label-free and no amplification and no modification in the assay process avoid other interferences. The high-resolution real-time signals for NADH and NAD^+ allow us to read out the information and simultaneously monitor their change.

We anticipate that the MC-nanopore tool can broadly apply in any involved-NAD^+/NADH biological processes and applications including the fundamental processes, such as

https://doi.org/10.1021/acs.analchem.1c00986
Anal. Chem. 2021, 93, 7118–7124

fuelling respiration, mediating cellular energy transduction,[34] the metabolism, unravelling the molecular details of the disease and therapy,[35,36] and detecting the balance and activity of over 500 related enzymes.[37] Furthermore, this paper provides a new strategy for developing the single-molecule technology.

■ ASSOCIATED CONTENT

Supporting Information

The Supporting Information is available free of charge at https://pubs.acs.org/doi/10.1021/acs.analchem.1c00986.

Experimental details describing the synthesis and characterization, detailed information on molecular simulation, and analysis of kinetics (PDF)

■ AUTHOR INFORMATION

Corresponding Author

Xiao-feng Kang − *Key Laboratory of Synthetic and Natural Functional Molecular Chemistry, College of Chemistry & Materials Science, Northwest University, Xi'an 710069, P. R. China*; orcid.org/0000-0002-2724-326X; Email: kangxf@nwu.edu.cn

Authors

Xingtong Liu − *Key Laboratory of Synthetic and Natural Functional Molecular Chemistry, College of Chemistry & Materials Science, Northwest University, Xi'an 710069, P. R. China*

Wanyue Feng − *Key Laboratory of Synthetic and Natural Functional Molecular Chemistry, College of Chemistry & Materials Science, Northwest University, Xi'an 710069, P. R. China*

Fujun Yao − *Key Laboratory of Synthetic and Natural Functional Molecular Chemistry, College of Chemistry & Materials Science, Northwest University, Xi'an 710069, P. R. China*

Jinlei Zhang − *Key Laboratory of Synthetic and Natural Functional Molecular Chemistry, College of Chemistry & Materials Science, Northwest University, Xi'an 710069, P. R. China*

Rauf Ayesha − *Key Laboratory of Synthetic and Natural Functional Molecular Chemistry, College of Chemistry & Materials Science, Northwest University, Xi'an 710069, P. R. China*

Tingting Chen − *Key Laboratory of Synthetic and Natural Functional Molecular Chemistry, College of Chemistry & Materials Science, Northwest University, Xi'an 710069, P. R. China*

Xiaoyu Shi − *Key Laboratory of Synthetic and Natural Functional Molecular Chemistry, College of Chemistry & Materials Science, Northwest University, Xi'an 710069, P. R. China*

Xixi Qiao − *Key Laboratory of Synthetic and Natural Functional Molecular Chemistry, College of Chemistry & Materials Science, Northwest University, Xi'an 710069, P. R. China*

Luping Ma − *Key Laboratory of Synthetic and Natural Functional Molecular Chemistry, College of Chemistry & Materials Science, Northwest University, Xi'an 710069, P. R. China*

Sha Yu − *Key Laboratory of Synthetic and Natural Functional Molecular Chemistry, College of Chemistry & Materials Science, Northwest University, Xi'an 710069, P. R. China*

Complete contact information is available at: https://pubs.acs.org/10.1021/acs.analchem.1c00986

Notes

The authors declare no competing financial interest.

■ ACKNOWLEDGMENTS

This work was financially supported by the National Science Foundation of China (NSFC: 21375104, 21327806, and 21874107).

■ REFERENCES

(1) Solomatin, S. V.; Greenfeld, M.; Herschlag, D. *Nat. Struct. Mol. Biol.* **2011**, *18*, 732−734.
(2) Cha, J.; Lee, I. *Exp. Mol. Med.* **2020**, *52*, 1798−1808.
(3) Wilkinson, D. J. *Nat. Rev. Genet.* **2009**, *10*, 122−133.
(4) Altamirano, M. M.; Blackburn, J. M.; Aguayo, C.; Fersht, A. R. *Nature* **2000**, *403*, 617−622.
(5) Biefer, H. R. C.; Elkhal, A.; Cesarovic, N.; Emmert, M. Y. *Eur. Heart J.* **2020**, *41*, 983−986.
(6) Imai, S.-i.; Guarente, L. *Trends Cell Biol.* **2014**, *24*, 464−471.
(7) Kim, W.; Deik, A.; Gonzalez, C.; Gonzalez, M. E.; Fu, F.; Ferrari, M.; Churchhouse, C. L.; Florez, J. C.; Jacobs, S. B. R.; Clish, C. B.; Rhee, E. P. *Cell Metab.* **2019**, *29*, 856−870.
(8) Berger, F. *Trends Biochem. Sci.* **2004**, *29*, 111−118.
(9) Rutter, J.; Reick, M.; Wu, C. L.; McKnight, S. L. *Science* **2001**, *293*, 510−514.
(10) Lautrup, S.; Sinclair, D. A.; Mattson, M. P.; Fang, E. F. *Cell Metab.* **2019**, *30*, 630−655.
(11) Verdin, E. *Science* **2015**, *350*, 1208−1213.
(12) Goodman, R. P.; Markhard, A. L.; Shah, H.; Sharma, R.; Skinner, O. S.; Clish, C. B.; Deik, A.; Patgiri, A.; Hsu, Y.-H. H.; Masia, R.; Noh, H. L.; Suk, S.; Goldberger, O.; Hirschhorn, J. N.; Yellen, G.; Kim, J. K.; Mootha, V. K. *Nature* **2020**, *583*, 122−126.
(13) Istrate, O.-M.; Rotariu, L.; Marinescu, V. E.; Bala, C. *Sens. Actuators, B* **2016**, *223*, 697−704.
(14) Baskar, S.; Chang, J.-L.; Zen, J.-M. *Biosens. Bioelectron.* **2012**, *33*, 95−99.
(15) Zhao, Y.; Hu, Q.; Cheng, F.; Su, N.; Wang, A.; Zou, Y.; Hu, H.; Chen, X.; Zhou, H.-M.; Huang, X.; Yang, K.; Zhu, Q.; Wang, X.; Yi, J.; Zhu, L.; Qian, X.; Chen, L.; Tang, Y.; Loscalzo, J.; Yang, Y. *Cell Metab.* **2015**, *21*, 777−789.
(16) Podder, A.; Koo, S.; Lee, J.; Mun, S.; Khatun, S.; Kang, H.-G.; Bhuniya, S.; Kim, J. S. *Chem. Commun.* **2019**, *55*, 537−540.
(17) Quah, T.; Milton, R. D.; Abdellaoui, S.; Minteer, S. D. *Chem. Commun.* **2017**, *53*, 8411−8414.
(18) Kang, X.-f.; Cheley, S.; Rice-Ficht, A. C.; Bayley, H. *J. Am. Chem. Soc.* **2007**, *129*, 4701−4705.
(19) Kang, X.-f.; Gu, L.-Q.; Cheley, S.; Bayley, H. *Angew. Chem., Int. Ed.* **2005**, *44*, 1495−1499.
(20) Derrington, I. M.; Butler, T. Z.; Collins, M. D.; Manrao, E.; Pavlenok, M.; Niederweis, M.; Gundlach, J. H. *Proc. Natl. Acad. Sci. U.S.A.* **2010**, *107*, 16060−16065.
(21) Tan, C. S.; Fleming, A. M.; Ren, H.; Burrows, C. J.; White, H. S. *J. Am. Chem. Soc.* **2018**, *140*, 14224−14234.
(22) Yao, F.; Peng, X.; Su, Z.; Tian, L.; Guo, Y.; Kang, X.-f. *Anal. Chem.* **2020**, *92*, 3827−3833.
(23) Guan, X.; Gu, L.-Q.; Cheley, S.; Braha, O.; Bayley, H. *ChemBioChem* **2005**, *6*, 1875−1881.
(24) Maglia, G.; Restrepo, M. R.; Mikhailova, E.; Bayley, H. *Proc. Natl. Acad. Sci. U.S.A.* **2008**, *105*, 19720−19725.
(25) Gu, L.-Q.; Cheley, S.; Bayley, H. *Proc. Natl. Acad. Sci. U.S.A.* **2003**, *100*, 15498−15503.
(26) Li, T.; Liu, L.; Li, Y.; Xie, J.; Wu, H.-C. *Angew. Chem., Int. Ed.* **2015**, *54*, 7568−7571.
(27) Wang, G.; Wang, L.; Han, Y.; Zhou, S.; Guan, X. *Biosens. Bioelectron.* **2014**, *53*, 453−458.

(28) Ho, C.-W.; Van Meervelt, V.; Tsai, K.-C.; De Temmerman, P.-J.; Mast, J.; Maglia, G. *Sci. Adv.* **2015**, *1*, No. e1500905.
(29) Ying, Y.-L.; Wang, H.-Y.; Sutherland, T. C.; Long, Y.-T. *Small* **2011**, *7*, 87−94.
(30) Su, Z.; Wei, Y.; Kang, X.-f. *Anal. Chem.* **2019**, *91*, 15255−15259.
(31) Ashton, P. R.; Königer, R.; Stoddart, J. F.; Alker, D.; Harding, V. D. *J. Org. Chem.* **1996**, *61*, 903−908.
(32) Kupis, W.; Pałyga, J.; Tomal, E.; Niewiadomska, E. *J. Physiol. Biochem.* **2016**, *72*, 371−380.
(33) Cantó, C.; Gerhart-Hines, Z.; Feige, J. N.; Lagouge, M.; Noriega, L.; Milne, J. C.; Elliott, P. J.; Puigserver, P.; Auwerx, J. *Nature* **2009**, *458*, 1056−1060.
(34) Luongo, T. S.; Eller, J. M.; Lu, M.-J.; Niere, M.; Raith, F.; Perry, C.; Bornstein, M. R.; Oliphint, P.; Wang, L.; McReynolds, M. R.; Migaud, M. E.; Rabinowitz, J. D.; Johnson, F. B.; Johnsson, K.; Ziegler, M.; Cambronne, X. A.; Baur, J. A. *Nature* **2020**, *588*, 174−179.
(35) Robson, A. *Nat. Rev. Cardiol.* **2021**, *18*, 307.
(36) Chaurasiya, A.; Garg, S.; Khanna, A.; Narayana, C.; Dwivedi, V. P.; Joshi, N.; e Anam, Z.; Singh, N.; Singhal, J.; Kaushik, S.; Kaur Kahlon, A.; Srivastava, P.; Marothia, M.; Kumar, M.; Kumar, S.; Kumari, G.; Munjal, A.; Gupta, S.; Singh, P.; Pati, S.; et al. *Cell Death Discovery* **2021**, *7*, 10.
(37) Jiang, Y.; Liu, T.; Lee, C.-H.; Chang, Q.; Yang, J.; Zhang, Z. *Nature* **2020**, *588*, 658−663.

https://doi.org/10.1021/acs.analchem.1c00986
Anal. Chem. 2021, 93, 7118−7124